Biointerphases
A Journal of Biomaterials and Biological Interfaces

ARTICLE

avs.scitation.org/journal/bip

Loss of membrane asymmetry alters the interactions of erythrocytes with engineered silica nanoparticles

Cite as: Biointerphases 15, 041001 (2020); doi: 10.1116/6.0000246
Submitted: 7 April 2020 · Accepted: 11 June 2020 ·
Published Online: 29 June 2020

Parnian Bigdelou,[1] Amid Vahedi,[2] Evangelia Kiosidou,[2] and Amir M. Farnoud[1,2,a)]

AFFILIATIONS

[1]Biomedical Engineering Program, Ohio University, Athens, Ohio 45701
[2]Department of Chemical and Biomolecular Engineering, Ohio University, Athens, Ohio 45701

[a)]**Electronic mail:** farnoud@ohio.edu

ABSTRACT

Disruption of plasma membrane integrity is a primary mechanism of nanoparticle toxicity in cells. Mechanistic studies on nanoparticle-induced membrane damage have been commonly performed using model membranes with a focus on symmetric bilayers, overlooking the fact that the membrane has an asymmetric phospholipid composition. In this study, erythrocytes with normal and scrambled membrane asymmetry were utilized to examine how the loss of membrane asymmetry and the resulting alterations in the outer leaflet lipid composition affect nanoparticle-membrane interactions. Unmodified, amine-modified, and carboxyl-modified silica (30 nm) were used as nanoparticle models. Loss of membrane asymmetry was achieved by induction of eryptosis, using a calcium ionophore. Erythrocyte membrane disruption (hemolysis) by unmodified silica nanoparticles was significantly reduced in eryptotic compared to healthy cells. Amine- and carboxyl-modified particles did not cause hemolysis in either cell. In agreement, a significant reduction in the binding of unmodified silica nanoparticles to the membrane was observed upon loss of membrane asymmetry. Unmodified silica particles also caused significant cell deformation, changing healthy erythrocytes into a spheroid shape. In agreement with findings in the cells, unmodified particles disrupted vesicles mimicking the erythrocyte outer leaflet lipid composition. The degree of disruption and nanoparticle binding to the membrane was reduced in vesicles mimicking the composition of scrambled membranes. Cryo-electron microscopy revealed the presence of lipid layers on particle surfaces, pointing to lipid adsorption as the mechanism for vesicle damage. Together, findings indicate an important role for the lipid composition of the membrane outer leaflet in nanoparticle-induced membrane damage in both vesicles and erythrocytes.

I. INTRODUCTION

The past two decades have witnessed an unprecedented increase in the use of engineered nanomaterials in industrial and biomedical applications. This has necessitated a better understanding of the mechanisms by which nanomaterials induce toxicity in mammalian cells. The plasma membrane, a lipid bilayer covering all cells, is the first cellular entity that comes into direct contact with exogenous nanoparticles. Studies in both membrane models and cells have shown that nanomaterials can disrupt membrane integrity, thereby leading to deleterious effects on cell viability.[1–7] It is thus important to investigate the underlying mechanisms by which nanoparticles disrupt membrane integrity and study how nanoparticle-induced membrane damage depends on nanoparticle and membrane properties.

The cell plasma membrane has an asymmetric phospholipid distribution. Phosphatidylcholine (PC) and sphingomyelin (SM) species are primarily localized in the outer leaflet, facing the outside environment,[8] while phosphatidylethanolamine (PE) and phosphatidylserine (PS) are predominantly in the inner leaflet, facing the cytoplasm.[9,10] Since its discovery in the 1970s,[11] membrane asymmetry has gained increasing attention in membrane biology and is known to regulate a variety of cellular functions including cell division, membrane fusion, apoptotic cell recognition, and clearance.[10,12] However, it has been largely overlooked in studies on nanoparticle-membrane interactions, leading to a lack of mechanistic information on whether the asymmetric distribution of lipids and the composition of each leaflet plays a role in nanoparticle-induced perturbations in the cell membrane.

Given the complexity of the plasma membrane, mechanistic studies on how nanomaterials disrupt membrane integrity are commonly performed using membrane models.[13] In a previous study[14] using lipid vesicles as a membrane model, we examined the role of membrane lipid asymmetry in the disruptive effects of silica nanoparticles, commonly used in industrial and biomedical applications,[15–18] on the membrane. This study, using symmetric and asymmetric vesicles, demonstrated that the lipid composition of the membrane outer leaflet plays an important role in the outcome of nanoparticle-membrane interactions with little to no effect from the inner leaflet. However, these findings were limited to lipid vesicles and could not be extended to live cells in which membrane complexity is significantly increased, due to the significant membrane lipid diversity, the presence of membrane proteins and carbohydrates, and the connection to the cell cytoskeleton.

Erythrocytes (red blood cells) are the most abundant cells in the bloodstream and one of the most commonly used cell models to examine membrane toxicity of nanomaterials.[19,20] Erythrocytes do not possess active endocytic machinery and nanoparticle toxicity in these cells is primarily associated with membrane damage. In addition, cell membrane disruption in erythrocytes can be easily tracked due to the efflux of hemoglobin (hemolysis). Like other mammalian cells, the phospholipids of the erythrocyte membrane are asymmetric.[21,22] However, certain clinical conditions trigger eryptosis, erythrocyte programmed death, resulting in the loss of phospholipid asymmetry and translocation of inner leaflet lipids to the outer leaflet.[23–25] Eryptosis can also be induced chemically using calcium ionophores,[25] allowing for examination of how the loss of membrane asymmetry and the subsequent alterations in the membrane outer leaflet affect nanoparticle-cell membrane interactions.

In this study, healthy and eryptotic erythrocytes were used to examine how the loss of membrane asymmetry and the resulting changes in the outer leaflet lipid composition affect nanoparticle-membrane interactions in cells. Eryptosis was induced by the calcium ionophore, ionomycin, and confirmed by the detection of the inner leaflet lipid, PS, in the outer leaflet. Unmodified, as well as amine- and carboxyl-modified silica nanoparticles (30 nm), were used to examine the role of nanoparticle surface chemistry in cell-nanomaterial interactions. Results show that loss of membrane asymmetry in erythrocytes leads to a dose-dependent reduction in nanoparticle binding to the membrane and nanoparticle-induced membrane disruption, although the effect is dependent on nanoparticle surface chemistry and is only observed in unmodified particles. Results were confirmed in vesicles mimicking each leaflet of the membrane, as well as scrambled membranes. Findings show that the composition of membrane outer leaflet plays an important role in nanoparticle binding to and disruption of the membrane in both vesicles and erythrocytes, although the effects are dependent on particle surface chemistry and the mechanisms of disruption are different in cells and vesicles.

II. MATERIALS AND METHODS

A. Materials

Deidentified human blood was commercially procured from ZenBio (Research Triangle, NC) in acid citrate dextrose (ACD) as the anticoagulant. Ionomycin calcium salt was procured from EMD Millipore (Burlington, MA). Annexin-V-Alexa Flour 488 conjugate and annexin-V binding buffer were purchased from Fisher Scientific. Fluorescein isothiocyanate (FITC)-conjugated unmodified, amine-modified, and carboxyl-modified silica nanoparticles (30 nm) were purchased from Micromod Partikeltechnologie GMBH (Rostock, Germany). Lipids, including 1,2-dioleoyl-sn-glycero-3-phosphocholine (DOPC), 1,2-dioleoyl-sn-glycero-3-phosphoethanolamine (DOPE), 1,2-dioleoyl-sn-glycero-3-phospho-L-serine (DOPS), brain sphingomyelin (SM), 1,2-dioleoyl-sn-glycero-3-phosphoethanolamine-*N*-(lissamine rhodamine B sulfonyl) (Rho-DOPE), and cholesterol (Chol) were procured from Avanti Polar Lipids (Alabaster, AL). Triton X-100, 5(6)-carboxyfluorescein (CF), glutaraldehyde, and osmium tetroxide solution were purchased from Sigma Aldrich (St. Louis, MO).

B. Induction of eryptosis

Induction of eryptosis was performed as we have recently reported.[25] Briefly, erythrocytes were isolated from whole blood by centrifugation at 700 g for 5 min and discarding the plasma and buffy coat. Cells were then washed two times in glucose-free Ringer solution containing 125 mM NaCl, 5 mM KCl, 1 mM $MgSO_4$, 32 mM [4-(2-hydroxyethyl)piperazin-1-yl]ethanesulfonic acid (HEPES), and 1 mM $CaCl_2$ (*p*H 7.4). Then, a 0.4% hematocrit suspension was prepared in glucose-free Ringer solution and incubated at 37 °C for 1, 3, 5, and 7 days to induce different levels of eryptosis. Afterward, erythrocyte membrane asymmetry was abolished by ionomycin in the presence of Ca^{2+}. Cells were treated with 1 μM ionomycin calcium salt in glucose-free Ringer solution for 2 h at 37 °C. Then, the cells were washed three times in glucose-free Ringer solution, centrifuged at 700 g for 5 min. The cell pellet was resuspended in annexin-V binding buffer. The cells were then incubated with annexin-V-Alexa Flour 488 conjugate for 20 min in the dark, washed with and resuspended in the binding buffer for flow cytometry measurements. Loss of membrane asymmetry was confirmed by monitoring the translocation of PS to the outer leaflet of the cell membrane. PS externalization was examined by monitoring the binding of annexin-V-Alexa-Fluor 488 to PS in the outer leaflet of cells. Flow cytometry was used to calculate the population of cells with scrambled membranes.

C. Characterization of silica nanoparticles

Unmodified, amine-modified, and carboxyl-modified silica nanoparticles (30 nm) were characterized for their size and charge using dynamic light scattering (DLS) and laser Doppler anemometry after dilution in PBS (pH 7.4) at a final concentration of 0.5 mg/ml (Table I). The DLS size was consistent with the nominal size of the nanoparticles. All particles were negatively charged due to the presence of silanol groups on their surface.

D. Nanoparticle-Induced disruption of erythrocytes

To study the hemolysis of healthy and eryptotic cells by silica nanoparticles, 0.05 mg/ml of unmodified, amine-, and carboxyl-modified silica nanoparticles were added to cells and incubated for 2 h at 37 °C to measure cell membrane disruption by silica

TABLE I. Hydrodynamic size and surface potential of engineered silica nanoparticles measured in PBS at a *p*H of 7.4.

Silica nanoparticles	Size (nm)	Charge (mV)
Unmodified	39.2 ± 10.3	−23.7 ± 2.8
Amine	38.0 ± 9.1	−13.1 ± 1.9
Carboxyl	38.0 ± 12.6	−16.2 ± 3.4

nanoparticles. After incubation, the cells were centrifuged at 700 g for 5 min, and the supernatant was collected. Hemolysis was examined by measuring the absorbance of oxygenated hemoglobin at 541 nm using a microplate reader and was calculated using the following equation:[14,25]

$$\%\text{Hemolysis} = (A_T - A_0)/(A_{100} - A_0)^*100. \quad (1)$$

Here, A_0 is the absorbance of erythrocytes in Ringer solution, A_{100} is the absorbance of erythrocytes in de-ionized water, and A_T is the absorbance of erythrocytes incubated with the silica nanoparticles. Note that for obtaining the absorbance value for A_{100}, de-ionized water was used to allow for the complete disruption of erythrocytes due to osmosis.

E. Nanoparticle binding to and internalization in erythrocytes

Flow cytometry was used to examine nanoparticle binding to and internalization in healthy and eryptotic erythrocytes.[26] Fluorescently labeled silica nanoparticles with different surface chemistries were added to erythrocytes at a final concentration of 0.001 mg/ml for 2 h of incubation at 37 °C. Lower concentration of nanoparticles (0.001 mg/ml) was used compared to hemolysis to prevent cell membrane disruption. Particle adhesion to the cell surface and internalization was measured by evaluating the fluorescence of nanoparticles using an excitation wavelength of 488 nm and an emission wavelength of 530 nm. To differentiate between the internalized and adhered particles, trypan blue, which is impermeable to healthy cells,[27] was used to quench the fluorescence of FITC-conjugated nanoparticles adhered to the cell surface.[28] The remaining fluorescence intensity corresponded to the nanoparticles internalized in the cells, as trypan blue is not permeable to the cell membrane and thus unable to quench the fluorescence of internalized particles.

F. Scanning electron microscopy

To observe the adherence of unmodified silica nanoparticles to healthy and eryptotic cells, 0.1 mg/ml unmodified particles were added to 1% hematocrit suspension and incubated for 2 h at 37 °C. After incubation, the cells were centrifuged at 700 g for 5 min, and the cell supernatant was removed. Then, the cells were washed two times in PBS, centrifuged at 700 g for 5 min, and the cell pellet was resuspended in 1 ml PBS. 1% glutaraldehyde was added dropwise to every 1 ml of the samples (healthy and eryptotic erythrocytes with and without nanoparticles) over the course of 5 min, and the samples were incubated at 37 °C for 1.5 h. Then, 1% osmium tetroxide was added to each sample and samples were incubated again for 1.5 h at 37 °C. Increasing concentrations of ethanol (50%, 60%, 70%, 80%, 90%, and 100%) were added to the cells for dehydration and incubated for 15 min at room temperature for each.[29] Droplets of the samples were added on glass coverslips and dried overnight. The samples were then coated with gold and observed under a scanning electron microscope. A JEOL JSM 6390LV scanning electron microscope (SEM) was used for the observation. The working distance was 15 mm, dictated by the configuration of the detectors inside the chamber. The accelerating voltage for best resolution was selected at 15 kV. All images presented were acquired using the secondary electrons detector. The spot size was in the range of 21–60 nm, depending on the magnification.

G. Vesicle leakage assay

Lipid vesicles mimicking outer (V_{outer}) and inner (V_{inner}) leaflets of the erythrocyte membrane and vesicles mimicking erythrocytes with scrambled lipids ($V_{scrambled}$) were synthesized, using the known lipid composition of the erythrocyte membrane leaflets.[14] V_{outer} lipid vesicles were synthesized using 44% Chol, 26% DOPC, 24% SM, and 6% DOPE, and V_{inner} lipid vesicles were composed of 44% Chol, 8% DOPC, 5% SM, 25% DOPE, and 18% DOPS.[11,14,30,31] $V_{scrambled}$ vesicles were synthesized using the average lipid composition of outer and inner leaflets: 44% Chol, 17% DOPC, 14.5% SM, 15.5% DOPE, and 9% DOPS. For the synthesis of lipid vesicles, different lipids were mixed to obtain 5 mM total lipid concentration in chloroform. The lipid mixtures were dried in a Speed Vac™ (ThermoFisher Scientific, Waltham, MA) and placed in a desiccator for at least 2 h to ensure complete drying. The self-quenching fluorescent probe, CF, was dissolved in PBS at a final concentration of 80 mM (*p*H 7.3) and added to the dried lipids at 70 °C. Vesicles were vortexed for 15 min and were subjected to seven cycles of freeze-thaw in acetone bath on dry ice and in a water bath at 70 °C, respectively, to ensure encapsulation of the dye. Large unilamellar vesicles were prepared by extruding the vesicles through a 100 nm polycarbonate filter (Avanti Polar Lipids) 11 times at 70 °C. Excess CF was removed by passing the vesicles through a PD-10 desalting column (Fisher Scientific, Hampton, NH).

For vesicle leakage studies, CF-encapsulated lipid vesicles eluted from the desalting column were diluted 200-fold in PBS to reach 25 μM final vesicle concentration and exposed to silica nanoparticles at a final concentration of 0.05 mg/ml in a 96-well plate. Triton X-100 was added to the lipid vesicles at 500-fold dilution and was used as the positive control of complete membrane disruption. Lipid vesicles in PBS were used as negative control. Leakage was examined by measuring the fluorescence intensity at 492/517 nm excitation/emission wavelengths, every 2.5 min over 1 h time course at 37 °C using a microplate reader, and was calculated according to the following equation:[14,25]

$$\%\text{Leakage} = (F_T - F_0)/(F_{100} - F_0)^*100. \quad (2)$$

Here, F_0 is the fluorescence intensity of vesicles in PBS, F_{100} is the fluorescence intensity of vesicles with Triton, and F_T is the fluorescence intensity of vesicles with the silica nanoparticles.

H. Nanoparticle binding to lipid vesicles

Nanoparticle binding to the lipid vesicles was studied using a fluorescence resonance energy transfer (FRET)-based assay as we have previously reported.[14,32] In this assay, Rho-DOPE, used as the FRET acceptor, was incorporated in lipid vesicles during the vesicle synthesis at a final concentration of 1 mo1. % of the total lipid content. Fluorescent nanoparticles (concentration of 0.05 mg/ml), used as FRET donors, were added to the lipid vesicles with (F sample) or without (F_0 sample) Rho-DOPE in their structure. Nanoparticles and vesicles were allowed to incubate for 2 h at 37 °C. At the end of incubation, the particle fluorescence intensity was measured using a plate reader at 485/515 nm excitation/emission wavelengths. Lipid vesicles without nanoparticles were used as negative control.

I. Cryo-transmission electron microscopy (CRYO-TEM) imaging of vesicles

Lipid vesicles mimicking the outer leaflet of erythrocyte membrane (V_{outer}) were prepared as described earlier. After seven freeze-thaw cycles, the vesicles were extruded through a 100 nm filter 33 times at 70 °C to obtain a high percentage of unilamellarity. Vesicles were then incubated with unmodified nanoparticles for 1 h, prior to freezing, at the same ratio used for the vesicle leakage assays. A small volume (3 μl) of the sample was added to a specimen grid. A period of 30–45 s was allowed for the sample to move toward the center of the grid before the automatic blotting of the excess liquid using the Thermo Scientific Vitrobot Mark IV system. The grid was immediately plunged into liquid ethane (cooled down with liquid nitrogen) after blotting to form a layer of amorphous ice. The grid was transferred to a Thermo Scientific Glacios CryoTEM (Thermo Fisher Scientific, Waltham, MA) under liquid nitrogen, and imaging was performed using Thermo Scientific Felcon direct electron detector. Electron microscopy was performed at the Center for Electron Microscopy and Analysis (CEMAS) at the Ohio State University.

III. RESULTS AND DISCUSSION

A. Characterization of eryptotic cells and nanoparticles

Eryptosis, programmed cell death in erythrocytes, was used to disrupt membrane lipid asymmetry in live erythrocytes. This process, which is similar to apoptosis in nucleated cells, results in scrambling of membrane asymmetry and translocation of the inner leaflet lipids to the outer leaflet.[23,33,34] Eryptosis was induced by preincubating the cells in glucose-free Ringer solution, followed by cell treatment with 1 μM ionomycin, as we have recently described.[25] Changes in the lipid composition of the membrane outer leaflet were confirmed using annexin-V staining, which detects PS in the outer leaflet.[35,36] The percentage of cells stained positively for annexin-V was measured using fluorescence-activated cell sorting (FACS) analysis and reported as percent eryptosis. Longer preincubation times in glucose-free Ringer solution resulted in a higher percentage of eryptotic cells, as evidenced by flow cytometry [Figs. 1(a)–1(d)]. Seven days of preincubation resulted in maximum eryptosis, as shown in Fig. 1(e).

Unmodified, carboxyl-modified, and amine-modified silica nanoparticles (nominal diameter = 30 nm) were examined for their interactions with healthy and eryptotic cells. The physicochemical properties of nanoparticles were characterized prior to the interaction experiments. Nanoparticle hydrodynamic diameter measured by dynamic light scattering was slightly larger than 30 nm but in close agreement with the nominal size. All particles were negatively charged due to the presence of silanol groups on their surface. Note that even the amine-modified particles remain negatively charged due to the abundance of silanol groups on the particle surfaces.

B. Nanoparticles show differences in hemolytic activity in cells with symmetric versus asymmetric membranes

To examine the disruptive effects of nanoparticles on the membrane of erythrocytes with symmetric and asymmetric membranes, unmodified, carboxyl-modified, and amine-modified silica particles were added to healthy and eryptotic erythrocytes. Studies were performed at a nanoparticle concentration of 0.05 mg/ml and a 0.4% hematocrit. Hemolytic effects of nanoparticles on erythrocytes are dose-dependent and the concentration of 0.05 mg/ml was selected, as it induced significant hemolysis in healthy cells, allowing for comparison between healthy and eryptotic cells.

Nanoparticle interactions with healthy and eryptotic cells were different but depended on particle surface properties (Fig. 2). In normal (asymmetric) cells, unmodified nanoparticles induced the highest degree of hemolysis (33.7 ± 0.9%). Note that hemolysis values are obtained from the absorbance of the released hemoglobin and are normalized to 100% hemolysis, which is the absorbance value obtained by complete hemolysis, achieved by exposing the cells to de-ionized water. The high hemolytic activity of silica particles is previously shown by us[14] and others[20,37–40] and is caused by ion-pairing between silanol in silica and trimethylammonium in PC and SM.[32] In contrast, amine- and carboxyl-modified particles showed little hemolytic activity in healthy cells, likely due to the coverage of silanol groups by covalently bound amine and carboxyl moieties. Loss of membrane asymmetry led to a significant reduction in the hemolytic activity of unmodified silica nanoparticles [Fig. 2(a)]. This effect was dose-dependent with the hemolysis decreasing with an increasing number of annexin-V binding cells. The degree of hemolysis induced in eryptotic cells by amine- and carboxyl-modified nanoparticles was higher than that observed in healthy cells but remained under 1% in all cases [Figs. 2(b) and 2(c)].

C. Nanoparticles bind differently to cells with symmetric versus asymmetric membranes

Nanoparticle-induced disruption of the plasma membrane requires that nanoparticles first bind to the bilayer. To understand why changes in lipid asymmetry have resulted in changes in the hemolytic activity of nanoparticles, nanoparticle binding to and internalization in healthy and eryptotic cells were evaluated. To this aim, flow cytometry was used to measure the fluorescence intensity of FITC-conjugated particles that bound to and internalized in healthy and eryptotic cells. Erythrocytes do not actively internalize nanomaterials; however, particles can passively diffuse through the erythrocyte membrane.[29] To distinguish membrane-bound from internalized nanoparticles, trypan blue quenching was used. Trypan blue does not permeate intact membranes;[27] thus, it only quenches

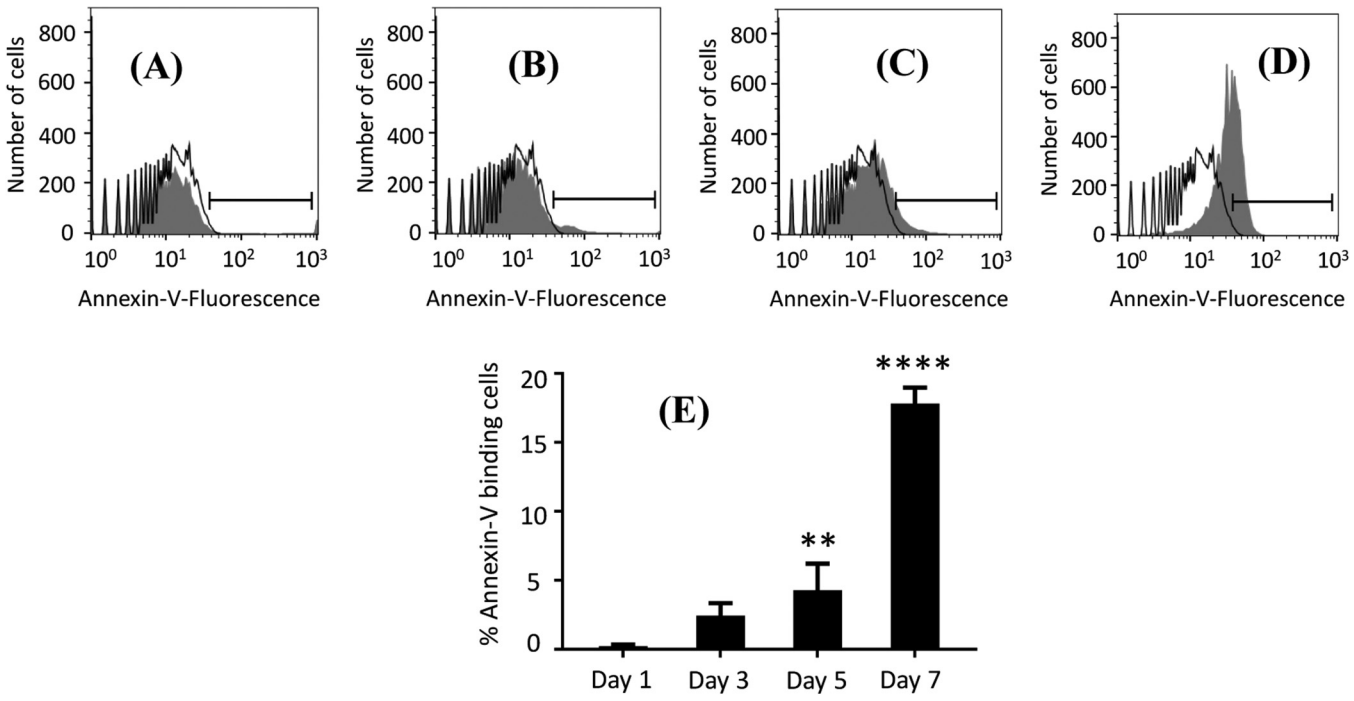

FIG. 1. Representative flow cytometry histograms for control erythrocytes (black) and erythrocytes treated with 1 μM ionomycin (gray) at 37 °C for 2 h at 0.4.% hematocrit, after preincubation in glucose-free Ringer solution for (a) 1, (b) 3, (c) 5, and (d) 7 days. The histogram marker is used to identify the annexin-V binding cell population (positive events), compared to control (negative event). (e) Arithmetic mean ± standard deviation (n = 3) of the percentage of annexin-V binding cells over time. The highest eryptosis was obtained after seven days of preincubation in glucose-free Ringer solution, followed by treatment with 1 μM ionomycin. One-way analysis of variance (ANOVA) with Dunnett's test was performed to compare the percentage of annexin-V binding cells on different days with the same percentage on day 1. ** denotes $p < 0.01$, and **** denotes $p < 0.0001$.

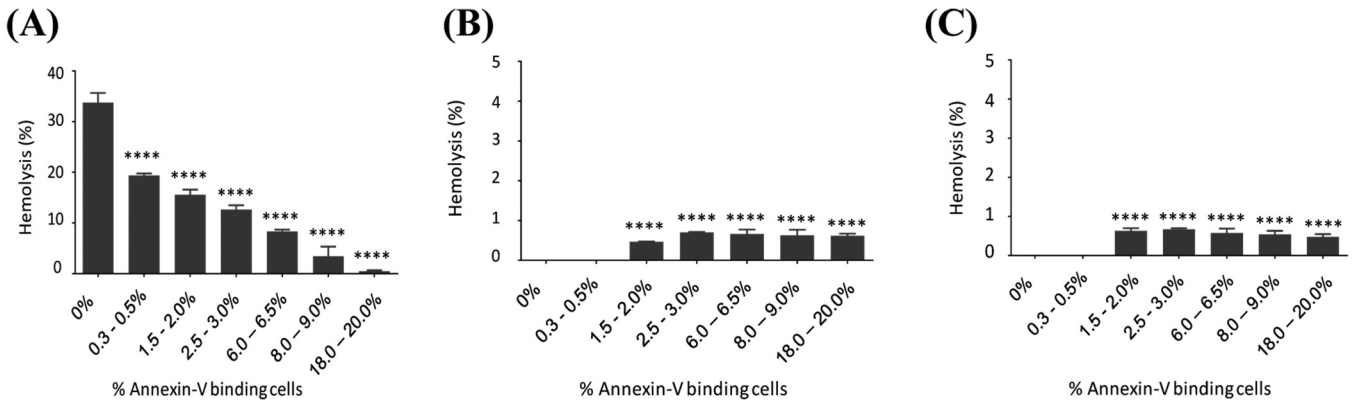

FIG. 2. Hemolysis of eryptotic erythrocytes by 0.05 mg/ml of (a) unmodified, (b) amine-, and (c) carboxyl-modified silica nanoparticles. To induce eryptosis, erythrocytes were incubated with 1 μM ionomycin at 37 °C for 2 h at 0.4% hematocrit, after preincubation in sugar-free Ringer solution for different time points. Zero percent of annexin-V binding indicates nontreated erythrocytes (negative control). One-way ANOVA with Dunnett's test was performed to compare the hemolysis percentage of eryptotic cells vs nontreated cells by nanoparticles. **** denotes $p < 0.0001$. Note that the maximum value of the y axis is different in panel (a), compared to panels (b) and (c).

the particles bound to the membrane. Note that a lower concentration of nanoparticles was used for these studies compared to the hemolysis experiments (0.001 vs. 0.05 mg/ml) to measure nanoparticle binding without complications from cell membrane disruption.

A significant difference in nanoparticle binding to normal and eryptotic cells was observed depending on particle surface chemistry. Unmodified silica particles showed significantly higher binding to and internalization in normal compared to eryptotic erythrocytes, as measured by the differences in the fluorescence intensity of internalized and bound nanoparticles in each set of cells [Figs. 3(a) and 3(d)]. This was in agreement with the reduced hemolytic activity of these nanoparticles toward eryptotic cells and suggested that scrambling of the membrane reduces the disruptive effects of nanomaterials by hampering their binding. In the case of amine- and carboxyl-modified nanoparticles, binding and internalization were similar between healthy and eryptotic cells [Figs. 3(c) and 3(f)]. Amine-modified particles showed a slightly higher binding and internalization in eryptotic compared to healthy cells. But, while statistically significant, the magnitude of the differences in fluorescence intensity was small. Overall, the minor differences in the membrane binding and internalization of amine- and carboxyl-modified nanoparticles upon changes in membrane asymmetry were consistent with the minor differences in the hemolytic activity of these particles in healthy versus eryptotic cells.

D. Nanoparticles deform the membrane of healthy cells

Having examined nanoparticle-induced membrane disruption and nanoparticle binding to the membrane, we then examined

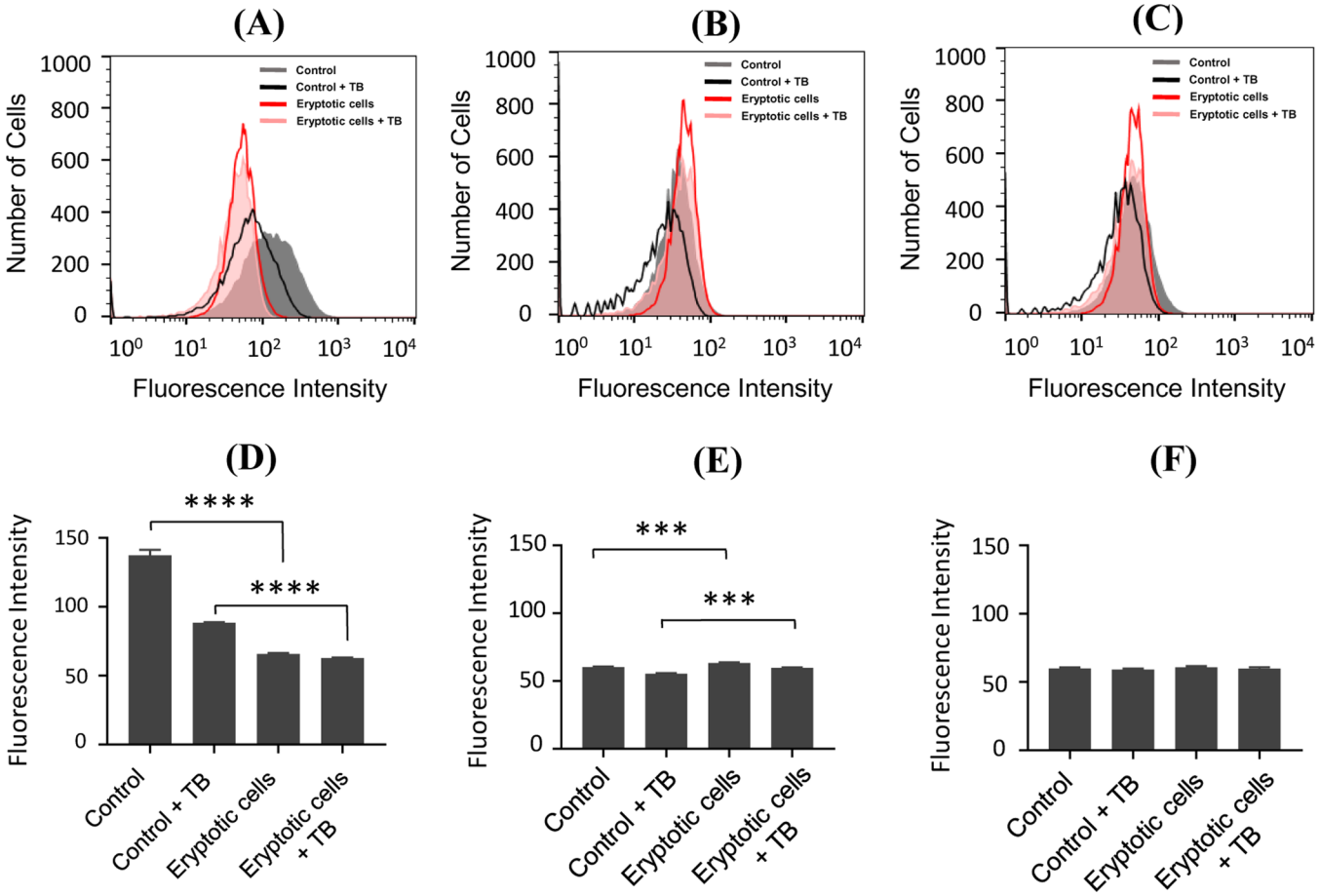

FIG. 3. Representative flow cytometry histograms for nanoparticle binding to and internalization in healthy and eryptotic erythrocytes for (a) unmodified, (b) amine-modified, and (c) carboxyl-modified silica nanoparticles, all at a concentration of 0.001 mg/ml. Gray histogram indicates bound and internalized nanoparticles in healthy erythrocytes. The black line indicates the internalized nanoparticles in healthy erythrocytes in the presence of trypan blue. The red line indicates adhered and internalized nanoparticles in eryptotic erythrocytes, and the pink histogram indicates the internalized nanoparticles in eryptotic cells in the presence of trypan blue. The arithmetic mean of median nanoparticle fluorescence intensity ± standard deviation (n = 3) in the presence and absence of trypan blue, are presented for (d) unmodified, (e) amine-modified, and (f) carboxyl-modified nanoparticles. T-test was performed to compare the fluorescence intensity of nanoparticles adhered to and internalized in healthy cells vs eryptotic cells. *** denotes $p < 0.001$ and **** denotes $p < 0.0001$.

nanoparticle-induced deformations in the cell membrane. Since unmodified silica nanoparticles had shown the highest hemolytic activity on both normal and eryptotic cells, studies were focused on these particles. For these studies, 0.1 mg/ml of unmodified silica nanoparticles were added to healthy and eryptotic erythrocytes for 2 h incubation at 37 °C, and the cells were observed under an SEM. In the absence of particles, healthy erythrocytes showed the disklike shape of normal cells [Fig. 4(a)], while eryptotic cells showed changes in cell surface morphology, as is expected from eryptotic cells [Fig. 4(b)].[33] Exposure of healthy erythrocytes to unmodified silica nanoparticles significantly affected their structure and resulted in their deformation into a more spheroid shape [Fig. 4(c)]. Some nanoparticle agglomerates could be found on the surface of erythrocytes (red arrows) although the SEM resolution is not high enough to separate out individual particles. It is also possible that some erythrocytes were completely hemolyzed as a result of the exposure, which could not be captured in the image. Interestingly, no significant change in the morphology of eryptotic cells was observed after exposure to nanoparticles [Fig. 4(d)]. A lower number of particle agglomerates could be found on the surface of eryptotic cells, which is consistent with the flow cytometry measurements, showing higher nanoparticle binding to healthy compared to eryptotic cells.

E. Nanoparticles disrupt vesicles mimicking each membrane leaflet differently

Eryptosis is associated with several changes in the cell, of which membrane scrambling is only a part.[41–44] Thus, from the studies in cells, it is not possible to pinpoint membrane scrambling as the main mechanism for the drastic differences in hemolysis by unmodified nanoparticles in healthy versus eryptotic cells. Studies in lipid vesicles were performed to confirm the role of membrane asymmetry. To this aim, vesicles mimicking the composition of the outer leaflet (V_{outer}), the inner leaflet (V_{inner}), and scrambled erythrocyte membranes ($V_{scrambled}$) were synthesized (see Sec. II for lipid composition of each vesicle). Then, the effect of nanoparticles on the integrity of these vesicles was examined using a vesicle leakage assay. In this assay, CF is encapsulated inside the vesicles at a high concentration (~80 mM), resulting in self-quenching. Nanoparticle-induced disruption of the vesicles will lead to the release of CF from the lumen of the vesicles, leading to its dilution below the self-quenching threshold, and a drastic increase in its fluorescence intensity (measured at 517 nm).

Nanoparticle interactions with V_{outer}, V_{inner}, and $V_{scrambled}$ lipid vesicles were different but depended on particle surface properties. Unmodified silica nanoparticles induced the highest degree of membrane leakage in the V_{outer} and lowest degree of membrane leakage in the V_{inner} vesicles [Fig. 5(a)]. Leakage of the $V_{scrambled}$ vesicles by unmodified nanoparticles was between that of the V_{outer} and the V_{inner} vesicles. These effects are consistent with the effects observed in erythrocytes, showing a reduction in hemolysis following membrane scrambling. Amine-modified and carboxyl-modified particles showed little membrane disruption in all lipid vesicles [Figs. 5(b) and 5(c)], although amine-modified nanoparticles were slightly more disruptive than carboxyl-modified nanoparticles. A likely explanation for this phenomenon could be a higher number of silanol groups on the surface of amine-modified particles. However, further nanoparticle characterization by silanol measurement, or using techniques such as x-ray photoelectron spectroscopy, could help better elucidate the mechanisms for such differences.

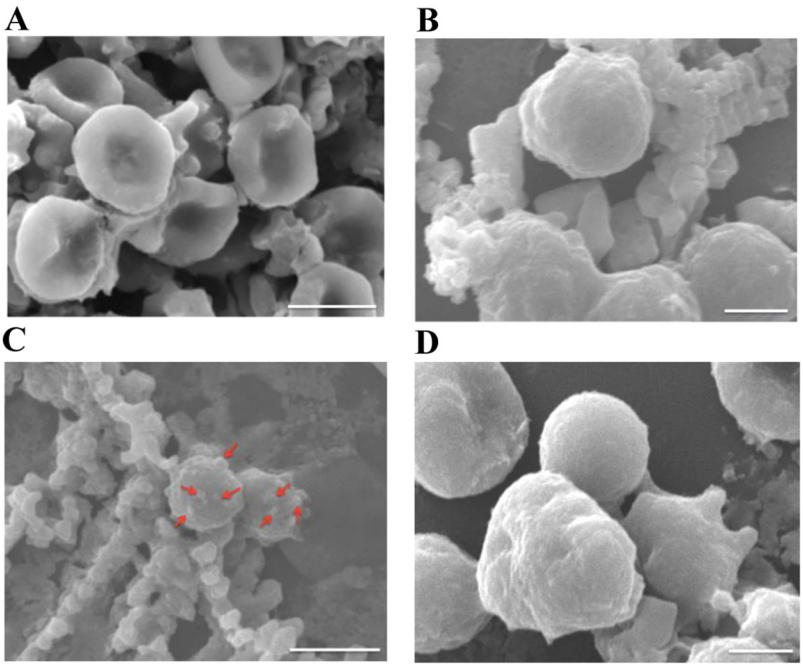

FIG. 4. Scanning electron microscopy images of (a) healthy and (b) eryptotic erythrocytes in the absence of nanoparticles, as well as (c) healthy and (d) eryptotic erythrocytes after exposure to unmodified silica nanoparticles (0.1 mg/ml) for 2 h. Red arrows in C indicate nanoparticle agglomerates on the surface of healthy erythrocytes. Scale bar is 5 μm in panels (a) and (c) and 2 μm in panels (b) and (d).

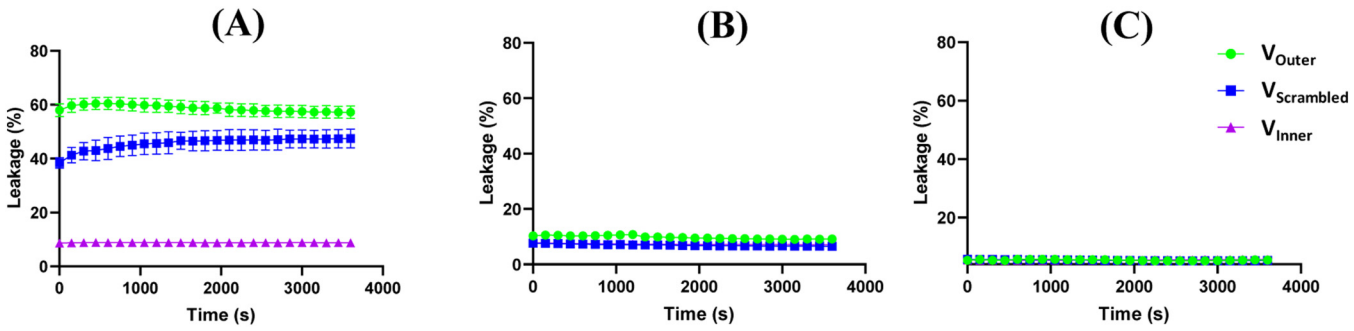

FIG. 5. Leakage of V_{outer}, V_{inner}, and $V_{scrambled}$ lipid vesicles (25 μM) following interaction with 0.05 mg/ml of (a) unmodified, (b) amine-, and (c) carboxyl-modified silica nanoparticles at 37 °C.

F. Nanoparticles bind differently to vesicles mimicking each membrane leaflet

The disruptive effects of nanoparticles on vesicles were further examined using a FRET-based assay that we have previously developed[14,32] to evaluate nanoparticle binding to the membrane. Rho-DOPE, which was incorporated in the lipid vesicles during their synthesis, was used as a FRET acceptor. When nanoparticles bind to the lipid vesicles, Rho-DOPE (FRET acceptor) quenches the fluorescence of FITC in nanoparticles (FRET donors) and the fluorescence intensity of FITC will decrease. Comparing the fluorescence intensity in the presence of the quencher (F) to the intensity in its absence (F_0) provides a quantitative measure for nanoparticle binding to vesicles. A low F/F_0 ratio indicates that a high level of nanoparticle binding, while a high F/F_0 indicates little to no binding (note that the maximum value of F/F_0 is one). All nanoparticles showed the lowest F/F_0 ratio in the V_{outer} vesicles and highest F/F_0 ratio in V_{inner} vesicles, suggesting increased binding to V_{outer} and comparatively lower binding to V_{inner}. Binding to the $V_{scrambled}$ vesicles was between that of V_{outer} and V_{inner} [Figs. 6(a)–6(c)]. Between the different particles, unmodified nanoparticles showed the highest binding to the lipid vesicles, which was consistent with them being more disruptive to the vesicles (and the cells).

G. Nanoparticles disrupt the vesicles by adsorbing lipids on their surface

Experiments in both erythrocytes and vesicles show that unmodified silica nanoparticles are more disruptive to membrane lipids compared to other particles. As we have recently described,

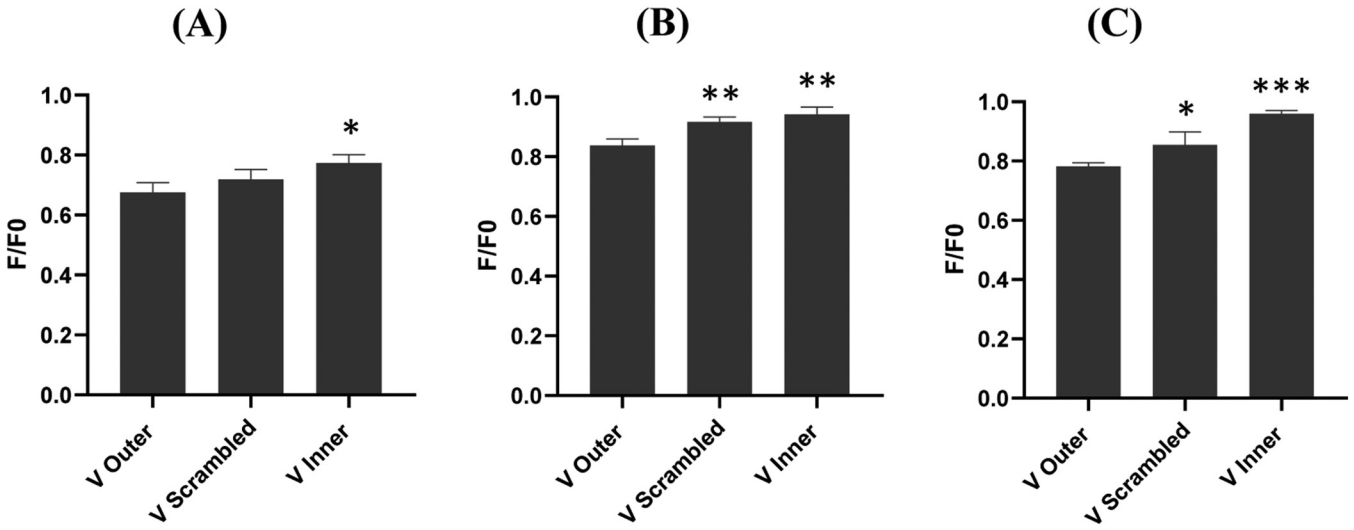

FIG. 6. Nanoparticle binding to the V_{outer}, V_{inner}, and $V_{scrambled}$ vesicles as a result of interaction with 0.05 mg/ml (a) unmodified, (b) amine-modified, and (c) carboxyl-modified silica nanoparticles. Note that F/F_0 inversely correlates to nanoparticle binding to the membrane. One-way ANOVA with Dunnett's test was performed to compare the nanoparticle binding to V_{inner} and $V_{scrambled}$ compared to V_{outer}. * denotes $p < 0.05$, ** denotes $p < 0.01$, and *** denotes $p < 0.001$.

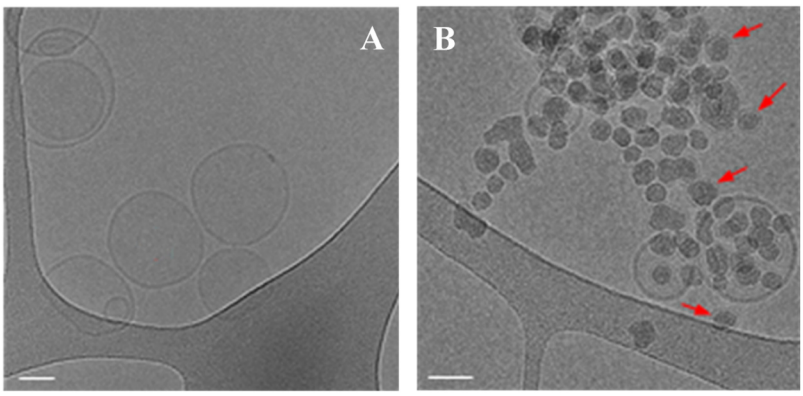

FIG. 7. Cryo-TEM images of the V_{outer} vesicles (a) before and (b) after 1 h of incubation with unmodified silica nanoparticles. Red arrows point to nanoparticles covered by lipids. The scale bar is 50 nm.

the disruptive effects of silica nanoparticles on PC and SM lipids, which are abundant in the V_{outer} vesicles, is due to ion-pairing between silanol in the particles and trimethylammonium in the headgroup of these lipids.[14,32] However, to understand whether nanoparticles deform the vesicles similar to erythrocytes, cryo-transmission electron microscopy (cryo-TEM) was used. Figure 7(a) shows the V_{outer} vesicles without incubation with nanoparticles. As can be seen in this image, even after multiple freeze-thaw cycles and extrusion, not all of the vesicles are unilamellar, as has been recently reported.[45] V_{outer} vesicles after 1 h of incubation with unmodified silica nanoparticles are shown in Fig. 7(b). In general, unlike erythrocytes, vesicles were not deformed after exposure to nanoparticles. However, nanoparticles were frequently found inside the vesicles with lipid bilayer or multilayers formed around them [Fig. 7(b), arrows]. This suggests that nanoparticles at least partially disrupted the vesicles by adsorbing membrane lipids on their surface. Given the comparable size of nanoparticles and vesicles, lipid adsorption on particles strips the vesicles of significant surface area, leading to their disruption as has been reported for a different vesicle system.[46]

H. Discussion

Despite increasing interest in understanding the mechanisms of nanoparticle-induced cell membrane damage, little attention has been paid to the fact that the plasma membrane is asymmetric with respect to its phospholipid composition. In previous work,[14] we had studied nanoparticle interactions with symmetric and asymmetric vesicles, demonstrating that the outer leaflet is the primary regulator of nanoparticle-induced membrane disruption in vesicles. Here, we expand these findings to live erythrocytes, demonstrating that the erythrocyte outer leaflet lipid composition regulates how nanomaterials disrupt the membrane of these cells, causing hemolysis. These results are not only important in the context of health implications of nanotechnology but can also pave the way for nanoparticle-based screening assays for diseases in which the composition of the membrane outer leaflet is altered.

Over the years, membrane models, such as lipid vesicles, have been highly valuable in understanding how nanomaterials disrupt biological membranes. However, while it is possible to easily change the lipid composition of membrane models, a common issue with all models is that they do not capture the complexities of the plasma membrane in live cells.[13] More information is emerging on how membrane proteins[47] and the cell cytoskeleton[48] affect nanoparticle interactions with the cell membrane. However, these important structural features cannot be captured in studies with lipid-based membrane models. In the current study, we utilized the well-known process of eryptosis to alter the lipid composition of the erythrocyte outer leaflet through membrane scrambling (Fig. 1). This process allows for examination of the role of loss of membrane asymmetry in nanoparticle-induced membrane disruption, in the presence of membrane proteins and cell cytoskeleton, which cannot be mimicked using membrane models.

Our results show that unmodified silica nanoparticles disrupt the membrane of healthy erythrocytes, with asymmetric membranes, more than eryptotic erythrocytes, with symmetric membranes (Fig. 2). Silica nanoparticles disrupt membranes containing PC and SM due to ion-pairing between silanol in silica and trimethylammonium in the headgroups of these lipids, which are abundant in the outer leaflet of erythrocytes.[11] Nanoparticle effects on healthy erythrocytes are highly dependent on particle surface chemistry and the differences in the hemolytic activity of unmodified and carboxyl-modified particles, with similar surface charge, are particularly interesting. We have recently shown that both particles bind to single-component vesicles containing phosphocholines.[32] In unmodified particles, binding occurs due to ion-pairing between silanol in silica and trimethylammonium in the choline headgroup. In carboxyl-modified particles, binding likely occurs through a similar electrostatic interaction between carboxyl and trimethylammonium; however, this interaction appears to be weaker and causes binding but not disruption.

Membrane scrambling results in the presence of aminophospholipids in the membrane outer leaflet and abrogates the disruptive effects of unmodified nanoparticles as well as particle binding to the membrane (Figs. 2 and 3). Importantly, these experiments were carried out in Ringer solution, in the absence of serum proteins, and with healthy and eryptotic erythrocytes, which had been thoroughly washed. Thus, it is unlikely that the lower amount of hemolysis in eryptotic cells is due to the binding of different proteins to the particle surfaces and the formation of a protein corona. Rather, such effects are caused due to a reduction in the level of PC and SM, and an increase in the level of PE and PS in the outer

leaflet. It should also be noted that while scrambling of the plasma membrane in eryptosis is well-established,[25,49–52] and the presence of PS in the outer leaflet was confirmed in the current study, the composition of other phospholipids in the outer leaflet has not been examined in the current study.

Findings on the nanoparticle-induced disruption of healthy and eryptotic cells were confirmed in vesicles. Unmodified nanoparticle showed significant binding to and disruption of vesicles mimicking the plasma membrane outer leaflet, which was reduced in scrambled membranes and vesicles mimicking the membrane inner leaflet (Figs. 5 and 6). While these results confirm the findings in cells and are consistent with our previous work,[14] one should use caution when comparing findings in vesicles to those in live cells. In addition to not containing membrane proteins, vesicles are also significantly smaller than cells (100 nm compared to several microns), resulting in a much lower membrane to nanoparticle surface area ratio than that observed in erythrocytes. While all the particles used in this study had a similar size (nominal diameter = 30 nm), it is worth noting that the relative particle and membrane size play an important role in the disruptive effects of particles. In general, larger particles are more disruptive to vesicles than smaller particles as their invagination in the vesicle can strip the vesicle of a larger membrane area.[46,53,54]

The qualitative agreement between the findings in cells and those in vesicles suggests that membrane outer leaflet lipid composition plays an important role in the outcome of interactions in both models. However, differences are also observed. For example, the difference in the leakage from the V_{outer} vesicles compared to the $V_{scrambled}$ vesicles is not as significant as what is observed between healthy and eryptotic cells. This could be due to differences in the outer leaflet lipid composition between the $V_{scrambled}$ vesicles and eryptotic cells. While $V_{scrambled}$ vesicles are simply an average of the outer and inner leaflet lipid composition, scrambling in eryptotic cells might not be the same for all lipids and could, for example, result in less PC and SM in the cell outer leaflet, than the average of both leaflets, thereby reducing the disruption by unmodified nanoparticles. A better characterization of the outer leaflet lipid composition of eryptotic erythrocytes is needed to explain the differences.

It is also important to consider some of the potential differences in the mechanism of nanoparticle-induced membrane disruption between the V_{outer} vesicles and healthy erythrocytes. SEM images in cells demonstrate significant restructuring of the membrane of healthy erythrocytes in the presence of particles and the presence of nanoparticle agglomerates on the cell surface (Fig. 4). Membrane bending by nanoparticles has been proposed as a mechanism by which silica nanoparticles disrupt erythrocytes[29] and is likely to be the case in the current study as evidenced by the significant changes in erythrocyte membrane morphology. While a significant portion of particles also enter the cells and in the process are covered by cell membrane lipids, this is unlikely to contribute significantly to membrane damage. This is because the portion of membrane lipids lost during this process is small in comparison to the large surface area of erythrocytes. Lack of drastic changes in membrane morphology and the reduced binding of nanoparticles in eryptotic cells suggest that the outer leaflet PC and SM are needed for nanoparticle binding and nanoparticle-induced membrane deformation. No significant membrane deformation is observed in the V_{outer} vesicles after exposure to nanoparticles (Fig. 7). However, in this case, nanoparticle internalization in vesicles leads to lipid adsorption on their surface. This loss of membrane lipids leads to significant vesicle disruption as the portion of lipids adsorbed on nanoparticle surfaces is a significant portion of the small vesicle surface area. Nanoparticle binding to the vesicles still requires outer leaflet lipids and is significantly reduced in the V_{inner} model without significant PC and SM. However, while the same lipid species mediate nanoparticle binding to both vesicles and cells, the mechanism of binding in each model is different.

IV. SUMMARY AND CONCLUSIONS

Nanoparticle-induced cell membrane disruption depends on the outer leaflet lipid composition in both vesicles and live erythrocytes. The presence of SM and PC in the membrane outer leaflet leads to significant binding of unmodified silica nanoparticles to the membrane, resulting in membrane disruption in both vesicles and erythrocytes. However, the presence of aminophospholipids in the outer leaflet reduces binding and disruption. While the same membrane lipids are responsible for nanoparticle binding, the mechanisms of nanoparticle-induced membrane disruption are likely to be different in each model. These results are important in understanding the health implications of nanomaterials to cells with different membrane lipid compositions or cells in which lipid composition is altered due to aging or disease.

ACKNOWLEDGMENTS

This work was supported by the National Science Foundation (NSF) (Grant No. CBET1903568) and the National Institutes of Health (Grant No. R15ES030140). Financial support from the Russ College of Engineering and Technology and the Department of Chemical and Biomolecular Engineering at Ohio University is also acknowledged. Electron microscopy was performed at the Center for Electron Microscopy and Analysis (CEMAS) at the Ohio State University.

REFERENCES

[1]N. Lewinski, V. Colvin, and R. Drezek, Small **4**, 1 (2008).
[2]H. Zhang *et al.*, J. Am. Chem. Soc. **134**, 38 (2012).
[3]F. Wang, F. Gao, M. Lan, H. Yuan, Y. Huang, and J. Liu, Toxicol. In Vitro **23**, 5 (2009).
[4]K. L. Chen and G. D. Bothun, Environ. Sci. Technol. **48**, 2 (2014).
[5]B. Y. Moghadam, W. C. Hou, C. Corredor, P. Westerhoff, and J. D. Posner, Langmuir **28**, 47 (2012).
[6]H. Shinto, T. Fukasawa, K. Yoshisue, M. Tezuka, and M. Orita, Adv. Powder Technol. **25**, 6 (2014).
[7]A. Panariti, G. Miserocchi, and I. Rivolta, Nanotechnol. Sci. Appl. **5**, 1 (2012).
[8]A. Gupta, T. Korte, A. Herrmann, and T. Wohland, J. Lipid Res. **61**, 2 (2020).
[9]D. L. Daleke, J. Lipid Res. **44**, 2 (2003).
[10]B. Fadeel and D. Xue, Crit. Rev. Biochem. Mol. **44**, 5 (2009).
[11]A. J. Verkleij, R. F. A. Zwaal, B. Roelofsen, P. Comfurius, D. Kastelijn, and L. L. M. van Deenen, BBA Biomembr. **323**, 2 (1973).
[12]M. Doktorova, F. A. Heberle, B. Eicher, R. F. Standaert, J. Katsaras, E. London, G. Pabst, and D. Marquardt, Nat. Protoc. **13**, 9 (2018).
[13]A. M. Farnoud and S. Nazemidashtarjandi, Environ. Sci. Nano **6**, 1 (2019).
[14]S. Nazemidashtarjandi and A. M. Farnoud, Environ. Sci. Nano **6**, 4 (2019).

[15]Z. Li, J. C. Barnes, A. Bosoy, J. F. Stoddart, and J. I. Zink, Chem. Soc. Rev. **41**, 7 (2012).
[16]S. Shi, F. Chen, and W. Cai, Nanomedicine **8**, 12 (2013).
[17]A. Bitar, N. M. Ahmad, H. Fessi, and A. Elaissari, Drug Discov. Today **17**, 20 (2012).
[18]Y. Wang *et al.*, Nanomed. Nanotechnol. **11**, 2 (2015).
[19]A. Barbul, K. Singh, L. Horev-Azaria, S. Dasgupta, T. Auth, R. Korenstein, and G. Gompper, ACS Appl. Nano Mater. **1**, 8 (2018).
[20]T. Yu, A. Malugin, and H. Ghandehari, ACS Nano **5**, 7 (2011).
[21]F. Kuypers, B. H. Lubin, M. Yee, P. Agre, P. F. Devaux, and D. Geldwerth, Blood **81**, 4 (1993).
[22]X. Tong, M. Moradipour, B. Novak, P. Kamali, S. O. Asare, B. L. Knutson, S. E. Rankin, B. C. Lynn, and D. Moldovan, J. Phys. Chem. B **123**, 39 (2019).
[23]E. Lang and F. Lang, Semin. Cell Dev. Biol. **39**, 35–42 (2015).
[24]S. Basu, D. Banerjee, S. Chandra, and A. Chakrabarti, Glycoconj. J. **27**, 9 (2010).
[25]P. Bigdelou and A. M. Farnoud, J. Vis. Exp. **155**, e60659 (2020).
[26]A. Lesniak, A. Salvati, M. J. Santos-Martinez, M. W. Radomski, K. A. Dawson, and C. Åberg, J. Am. Chem. Soc. **135**, 4 (2013).
[27]K. Mascotti, J. McCullough, and S. R. Burger, Transfusion **40**, 6 (2000).
[28]S. Sahlin, J. Hed, and I. Runfquist, J. Immunol. Methods **60**, 2 (1983).
[29]Y. Zhao, X. Sun, G. Zhang, B. G. Trewyn, I. I. Slowing, and V. S. Y. Lin, ACS Nano **5**, 2 (2011).
[30]M. Garnier, J. R. Attali, P. Valensi, E. Delatour-Hanss, F. Gaudey, and D. Koutsouris, Metabolism **39**, 8 (1990).
[31]K. Leidl, G. Liebisch, D. Richter, and G. Schmitz, Biochim. Biophys. Acta Mol. Cell Biol. Lipids **1781**, 10 (2008).
[32]S. Nazemidashtarjandi, A. Vahedi, and A. M. Farnoud, Langmuir **36**, 18 (2020).
[33]E. Pretorius, J. N. Du Plooy, and J. Bester, Cell. Physiol. Biochem. **39**, 5 (2016).
[34]M. Briglia, M. A. Rossi, and C. Faggio, Curr. Med. Chem. **24**, 9 (2017).
[35]J. F. Tait, D. Gibson, and K. Fujikawa, J. Biol. Chem. **264**, 14 (1989).
[36]H. A. M. Andree, C. P. M. Reutelingsperger, R. Hauptmann, H. C. Hemker, W. T. Hermens, and G. M. Willems, J. Biol. Chem. **265**, 9 (1990).
[37]I. I. Slowing, C. W. Wu, J. L. Vivero-Escoto, and V. S. Y. Lin, Small **5**, 1 (2009).
[38]Z. Ma, J. Bai, Y. Wang, and X. Jiang, ACS Appl. Mater. Interfaces **6**, 4 (2014).
[39]A. J. Paula, D. S. T. Martinez, R. T. A. Júnior, A. G. S. Filho, and O. L. Alves, J. Braz. Chem. Soc. **23**, 10 (2012).
[40]Y. S. Lin and C. L. Haynes, J. Am. Chem. Soc. **132**, 13 (2010).
[41]F. Lang, E. Lang, and M. Fller, Transfus. Med. Hemother. **39**, 5 (2012).
[42]F. Lang, E. Gulbins, H. Lerche, S. M. Huber, D. S. Kempe, and M. Föller, Cell. Physiol. Biochem. **22**, 6 (2008).
[43]K. S. Lang, P. A. Lang, C. Bauer, C. Duranton, T. Wieder, S. M. Huber, and F. Lang, Cell. Physiol. Biochem. **15**, 5 (2005).
[44]F. Lang and S. M. Qadri, Blood Purif. **33**, 3 (2012).
[45]H. L. Scott, A. Skinkle, E. G. Kelley, M. N. Waxham, I. Levental, and F. A. Heberle, Biophys. J. **117**, 8 (2019).
[46]O. Le Bihan *et al.*, J. Struct. Biol. **168**, 3 (2009).
[47]E. S. Melby *et al.*, Langmuir **34**, 36 (2018).
[48]A. Aalipour, A. M. Xu, S. Leal-Ortiz, C. C. Garner, and N. A. Melosh, Langmuir **30**, 41 (2014).
[49]L. A. Barber, M. B. Palascak, C. H. Joiner, and R. S. Franco, Br. J. Haematol. **146**, 4 (2009).
[50]S. Gil-Parrado *et al.*, J. Biol. Chem. **277**, 30 (2002).
[51]D. L. Bratton, V. A. Fadok, D. A. Richter, J. M. Kailey, L. A. Guthrie, and P. M. Henson, J. Biol. Chem. **272**, 42 (1997).
[52]R. Chandra, P. C. Joshi, V. K. Bajpai, and C. M. Gupta, BBA Biomembr. **902**, 2 (1987).
[53]H. I. Alkhammash, N. Li, R. Berthier, and M. R. R. De Planque, Phys. Chem. Chem. Phys. **17**, 15547–15560 (2015).
[54]S. Zhang, A. Nelson, and P. A. Beales, Langmuir **28**, 35 (2012).